^{18}F-FDG Uptake Assessed by PET/CT in Abdominal Aortic Aneurysms Is Associated with Cellular and Molecular Alterations Prefacing Wall Deterioration and Rupture

Audrey Courtois[1], Betty V. Nusgens[1], Roland Hustinx[2], Gauthier Namur[2], Pierre Gomez[3], Joan Somja[4], Jean- Olivier Defraigne[5], Philippe Delvenne[4], Jean-Baptiste Michel[6], Alain C. Colige*[1], and Natzi Sakalihasan*[5]

[1]Laboratory of Connective Tissues Biology, GIGA-R, University of Liège, Sart-Tilman, Belgium; [2]Department of Nuclear Medicine, CHU Liège, University of Liège, Sart-Tilman, Belgium; [3]Department of Nuclear Medicine, CHC St. Joseph, Liège, Belgium; [4]Department of Anatomopathology, CHU Liège, GIGA, University of Liège, Sart-Tilman, Belgium; [5]Department of Cardiovascular and Thoracic Surgery, CHU Liège, University of Liège, Sart-Tilman, Belgium; and [6]INSERM U698, Hemostasis, Bio-engineering and Cardiovascular Remodelling, CHU Bichat, University Paris 7, Paris, France

Rupture of abdominal aortic aneurysms (AAAs) leads to a significant morbidity and mortality in aging populations, and its prediction would be most beneficial to public health. Spots positive for uptake of ^{18}F-FDG detected by PET are found in 12% of AAA patients (PET+), who are most often symptomatic and at high rupture risk. Comparing the ^{18}F-FDG–positive site with a negative site from the same aneurysm and with samples collected from AAA patients with no ^{18}F-FDG uptake should allow the discrimination of biologic alterations that would help in identifying markers predictive of rupture. **Methods**: Biopsies of the AAA wall were obtained from patients with no ^{18}F-FDG uptake (PET0, $n = 10$) and from PET+ patients ($n = 8$), both at the site positive for uptake and at a distant negative site of the aneurysmal wall. Samples were analyzed by immunohistochemistry, quantitative real-time polymerase chain reaction, and zymography. **Results:** The sites of the aneurysmal wall with a positive ^{18}F-FDG uptake were characterized by a strikingly increased number of adventitial inflammatory cells, highly proliferative, and by a drastic reduction of smooth muscle cells (SMCs) in the media as compared with their negative counterpart and with the PET0 wall. The expression of a series of genes involved in the maintenance and remodeling of the wall was significantly modified in the negative sites of PET+, compared with the PET0 wall, suggesting a systemic alteration of the aneurysmal wall. Furthermore, a striking increase of several matrix metalloproteinases (MMPs), notably the MMP1 and MMP13 collagenases, was observed in the positive sites, mainly in the adventitia. Moreover, PET+ patients were characterized by a higher circulating C-reactive protein. **Conclusion:** Positive ^{18}F-FDG uptake in the aneurysmal wall is associated with an active inflammatory process characterized by a dense infiltrate of proliferating leukocytes in the adventitia and an increased circulating C-reactive protein. Moreover, a loss of SMC in the media and alterations of the expression of genes involved in the remodeling of adventitia and collagen degradation potentially participate in the weakening of the aneurysmal wall preceding rupture.

Key Words: positron emission tomography; aneurysm; inflammation; metalloproteinases; rupture

J Nucl Med 2013; 54:1740–1747
DOI: 10.2967/jnumed.112.115873

Rupture of abdominal aortic aneurysms (AAAs) is the 13th leading cause of death in western society. Because AAA is generally asymptomatic, the prediction of its rupture risk is essential. The AAA diameter is the most usual predictive factor for the risk of rupture (*1,2*), and surgery is recommended when the maximum diameter is greater than 55 mm. Nevertheless, the evolution of AAA is staccato and highly unpredictable (*2,3*). In the current practice, a conservative approach is often considered for patients with small AAAs. However, small AAAs may also rupture at a rate varying from 8% to 2% according to the most recent literature (*4,5*), and many undiscovered aneurysms may grow to a considerable size without rupture. The aneurysm size is therefore not a fully reliable and specific parameter to evaluate the risk of rupture, an event that occurs when the resistance of the dilating arterial wall becomes too weak for sustaining the hemodynamic stress of the circulation.

The remodeling of the wall leading to the expansion and rupture of AAAs is characterized by extracellular matrix proteolysis, medial smooth muscle cell (SMC) rarefaction, and chronic local extravasation of leukocytes. The inflammatory infiltrates consist mostly of lymphocytes and phagocytes (*1*) and predominate in the adventitia (*6*). Among the enzymes involved in AAA progression, matrix metalloproteinases (MMPs) have been largely involved in elastin and collagen degradation, leading to the remodeling of the wall, its expansion (*7,8*), and ultimately rupture (*9*). Furthermore, the rupture site is characterized by a higher proteolytic activity (*10,11*), forming a gradient from the rupture edge to distal site as we previously showed (*12*).

^{18}F-FDG PET/CT is currently used to detect hypermetabolic activity of cells as seen in tumoral and inflammatory processes. Furthermore, several studies have shown that ^{18}F-FDG PET can reliably detect leukocyte activities in atherosclerosis (*13,14*). We previously reported that a focal uptake of ^{18}F-FDG was observed in patients with large, rapidly expanding or symptomatic aneurysms that are prone to rupture (*15*). Moreover, the anatomic site

Received Oct. 22, 2012; revision accepted May 7, 2013.
For correspondence or reprints contact: Audrey Courtois, Laboratory of Connective Tissues Biology, GIGA, University of Liège, Tour de Pathologie, B23/+3, B-4000 Sart-Tilman, Belgium.
E-mail: A.Courtois@student.ulg.ac.be
*Contributed equally to this work.
Published online Sep. 5, 2013.

with a positive ^{18}F-FDG uptake corresponded in some cases with the site of rupture (*16*). More recently, preliminary studies demonstrated that the regions displaying an ^{18}F-FDG uptake were enriched in leukocytes (*17,18*). All these data suggest that functional imaging such as PET/CT may be helpful to monitor AAA progression and may become a predictive tool for evaluating the rupture risk.

In this study, samples from the positive ^{18}F-FDG uptake site and from a distant negative site were collected from the same aneurysm. This approach allowed for the first time, to our knowledge, a paired comparison in an aneurysm growing in a single background of intrinsic and environmental factors. These paired biopsies were further compared with samples collected from AAA patients with no ^{18}F-FDG uptake, allowing the discrimination of biologic alterations associated with ^{18}F-FDG uptake that would help in identifying relevant biologic markers predictive of rupture.

MATERIALS AND METHODS

Patients and PET/CT Image Acquisition

The study was approved by the Liège University ethics committee, and written consent was obtained from all patients. PET/CT data were acquired in patients referred to our department for AAA diagnosed by ultrasound, using a Gemini BB (16-slide CT scanner; Philips) or a Discovery LS (16-slide CT scanner; GE Healthcare) according to our usual protocol (i.e., 60 min after injection of ^{18}F-FDG in patients who fasted for 6 h). The detailed protocol is described in the supplemental data (supplemental materials are available at http://jnm.snmjournals.org). Superimposed CT and PET images were first analyzed visually by 2 of the authors and classified as positive when focal or segmental ^{18}F-FDG uptake was observed. Regions of interest were then placed over the abnormal focus or the normal aortic wall, depending on the case and on the normal liver, to measure the maximum pixel value standardized uptake values (SUVmax). Because the standardized uptake values (SUVs) may vary depending on the PET/CT device and protocol, we elected to express the results as AAA–to–liver activity ratios (rSUV), with patients acting as their own control. We have validated this approach in other indications of ^{18}F-FDG PET/CT such as inflammatory diseases (*19*), and the liver was chosen as a reference tissue because its uptake has been shown to display a low within-patient variability in test–retest studies (*20*). Patients with known connective tissue disorders or thoracoabdominal aortic aneurysms were excluded from the study.

Among the 18 patients enrolled in this study, 10 had no ^{18}F-FDG uptake (PET0) and 8 had a positive uptake of ^{18}F-FDG (PET+). Patient demographic information is presented in Table 1. AAA size, deciding factors for elective surgery, rSUV, and time between PET and surgery are individually listed in Table 2.

Tissue Collection

Surgery was performed within an average time of 18 (PET0) and 19 (PET+) days after PET/CT (Table 2). In PET0 patients, a surgical biopsy was collected in the anterior aneurysmal wall. For PET+ patients, a fragment was collected at the site of ^{18}F-FDG uptake (positive site) localized using anatomic landmarks and CT images as illustrated in the supplemental data (Supplemental Fig. 1). A second fragment was taken at a distant site with no ^{18}F-FDG uptake (negative site, Fig. 1). In 6 of the 8 PET+ patients, the negative site could be collected in the anterior aneurysmal wall similarly to the PET0 patients, and for 2 patients it was collected in the lateroanterior wall. A full-thickness slice of these samples was fixed in 4% paraformaldehyde for histologic and immunohistochemical analysis. The media and adventitia of the remaining tissue were then separated, cut into small pieces, and snap-frozen in liquid nitrogen until use for transcriptomic and zymography analysis. The various analytic procedures were applied to these biologic samples as listed in Supplemental Table 1 for each patient.

TABLE 1
Characteristics of Patients with No ^{18}F-FDG Uptake (PET0) and with Positive ^{18}F-FDG Uptake (PET+)

Patient characteristic	PET0 (n = 10)	PET+ (n = 8)
Age (y)		
Median	75	78
IQR	71–80	69–81
Body mass index (kg/m^2)		
Median	26.1	25.2
IQR	24.0–28.7	23.0–27.7
Deciding factor for surgery		
Size ≥ 55 mm	8	2
Growth/pain	1	4
Anxiety	1	2
Sex distribution		
Male	10	6
Female	0	2
Cardiovascular events	6	1
Hypertension	8	4
Smoker		
Current	3	3
Former	5	4
COPD	5	4
Diabetes	1	0
Hyperlipidemia	6	4
Statins	8	4
β-blocker	5	2
Calcium channel blocker	3	2
ACEI	2	0
NSAID	0	2

IQR = interquartile range; COPD = chronic obstructive pulmonary disease; ACEI = angiotensin-converting enzyme inhibitor; NSAID = nonsteroidal antiinflammatory drug.

Sample Analyses

Complete analytic and semiquantification procedures are detailed in the supplemental data. Briefly, paraffin-embedded sections of AAA specimens were stained with hematoxylin and eosin (H/E). SMCs and leukocytes were stained using specific antibodies against, respectively, α-smooth muscle actin (α-SMA) and CD45, CD3, CD20, CD68, and CD138. Proliferating cells were labeled by an anti-Ki67 antibody.

RNA was isolated from liquid nitrogen–pulverized tissue samples using Trizol or the RiboPure kit (Ambion) and its quality assessed by the Experion Automated Electrophoresis System (Bio-Rad). Only samples with an RNA quality indicator greater than 7 were included in the study (Supplemental Table 1). Gene expression was measured by semiquantitative RT polymerase chain reaction (PCR) or by real-time PCR using the oligonucleotides detailed in Supplemental Table 2.

Proteins were extracted in 2 M urea buffer from ground tissues, and zymography was performed as previously described (*7*).

Statistical Analysis

Results were expressed as the median and the interquartile range and considered to be significant at the 5% critical level ($P < 0.05$) using the Mann–Whitney U test for unpaired samples or the Wilcoxon signed-rank test for paired samples. Correlations between inflammatory cell density and SUV were established using the Spearman test for nonparametric values.

TABLE 2
Clinical Features of Patients With or Without ^{18}F-FDG Uptake in Aneurysmal Wall

Patient no.	Deciding factor	AAA size (mm)	rSUV	Time between PET and surgery (d)
No ^{18}F-FDG uptake				
1	≥55 mm	67	0.58	20
2	≥55 mm	70	0.33	4
3	≥55 mm	60	0.33	5
4	≥55 mm	55*	0.41	36
5	≥55 mm	57*	0.18	18
6	Growth	54†	0.54	6
7	≥55 mm	80*	0.76	28
8	≥55 mm	56	0.43	8
9	Anxiety	53	0.58	26
10	≥55 mm	71	0.70	18
Median		58.5	0.49	18
IQR		55.3–69.3	0.35–0.58	7–25
Positive for ^{18}F-FDG uptake				
11	Anxiety	52	1.04	44
12	Growth	54	0.89	7
13	Pain	40*	1.93	19
14	Growth	55	1.22	28
15	≥55 mm	69	1.06	20
16	≥55 mm	67	0.89	5
17	Anxiety	57	0.97	21
18‡	Growth	53	0.84	11
Median		54.5	1.00§	19
IQR		52.8–59.5	0.89–1.10	10–23

*Neoplasia.
†Renal insufficiency.
‡Diffuse uptake.
§$P < 0.001$, Mann-Whitney *U* test.
rSUV = aortic SUVmax/liver SUVmax. IQR = interquartile range.

RESULTS

PET/CT Data, Patient Demographics, and Clinical Features

Among the 18 patients enrolled in this study, 10 did not show any significant uptake of ^{18}F-FDG (PET0) whereas 8 presented an uptake (PET+) in the aneurysmal wall. In most cases, the uptake appeared as a focal zone in the wall (Fig. 1), was never localized in the neck of the aneurysm, and was not detected in the thrombus, when present. No significant difference in the median age and body mass index was noted between the 2 groups (Table 1). The male sex predominated in both groups, and the proportion of patients with a smoking habit and chronic obstructive pulmonary disease was similar. As individually listed in Table 2, 8 of the 10 patients in the PET0 group were asymptomatic, and the deciding factor for elective surgery was an aneurysm size of 55 mm or greater. Only 1 patient in this group (patient 6) presented a significant expansion rate (8 mm in 12 mo). By contrast, among the 8 patients of the PET+ group, 3 were operated on because of accelerated growth rate, 1 for pain, only 2 for an aneurism size of 55 mm or greater, and 2 for anxiety reasons. The time between PET and surgery was similar in both groups. The median diameter of AAA was also similar in both groups.

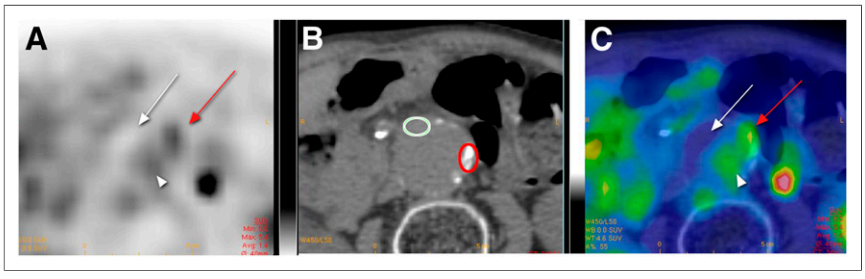

FIGURE 1. Example of positive ^{18}F-FDG PET/CT: transaxial PET (A), CT (B), and fused PET/CT images (C). Focus of increased activity is visible in left lateral aspect of aortic wall (red arrow). SUVmax is 5.4 at this level and 2.8 in liver (not shown). There is absence of uptake by thrombus (white arrow) and mild uptake by intraaortic blood pool (arrowhead). Red circle indicates tissue sampling during surgery in positive site and white circle in negative site after procedure of anatomic localization described in detail in supplemental data (Supplemental Fig. 1).

The metabolic activity in the AAA expressed as the rSUV (AAA/liver) was significantly higher in the PET+ patients than in PET0 patients (Table 2), thus corroborating the visual evaluation of the PET/CT image. No significant correlation was found between AAA diameter and rSUV. The preoperative level of circulating C-reactive protein (CRP) was significantly increased in the PET+ group as compared with the PET0 patients (Fig. 2).

Tissue Organization

Two sections distant of 100 μm from each PET0 and negative and positive site

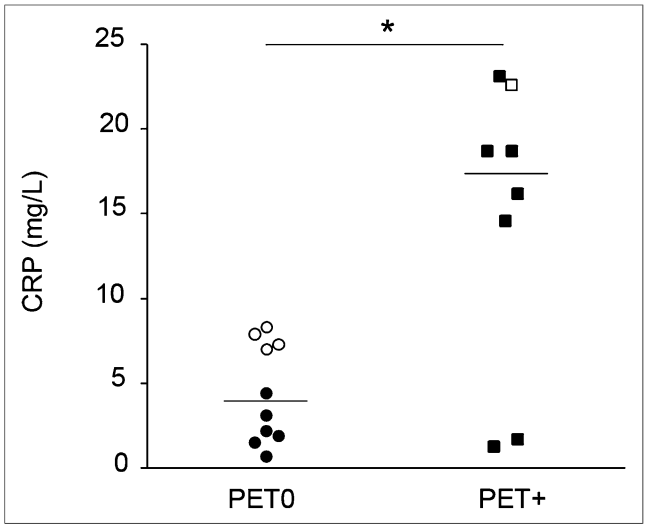

FIGURE 2. Preoperative circulating CRP: median concentration (mg/L) in PET0 patients (● = PET0 without comorbidity and ○ = PET0 with comorbidity as listed in Table 2) and in PET+ patients (■ = PET+ without comorbidity and □ = PET+ with comorbidity). *$P < 0.01$, Mann–Whitney U test.

of PET+ AAA were stained with H/E (Fig. 3A). An inflammatory infiltrate was present in the wall, mainly in the adventitia, and most prominent in the ^{18}F-FDG–positive sites (Fig. 3A, bottom) as compared with the negative site in the same patient (Fig. 3A, middle) and with the PET0 wall (Fig. 3A, top). The massive infiltrate in the positive sites was sometimes organized in tertiary lymphoid organs (Fig. 3A, arrow, bottom). A score was established in both series of H/E-stained samples by computer-assisted image analysis. The median score of the positive sites (Table 3) was significantly higher than their respective negative counterparts or than the PET0 samples. The number of neutrophils, counted in the same H/E-stained sections, was low, 5–10 per microscopic field, whatever the sample category.

Serial sections of the same samples were immunostained for markers of SMCs (α-SMA) (Fig. 3B) and proliferating cells (Ki67) (Fig. 3C). The density of α-SMA–positive cells was significantly reduced (2-fold) in the positive ^{18}F-FDG uptake sites (Fig. 3B, bottom; Table 3) as compared with their respective negative counterparts (Fig. 3B, middle) and with the PET0 patients (Fig. 3B, top). A significantly higher number of proliferating cells was observed in the positive sites (Fig. 3C, bottom; Table 3) as compared with the negative sites of PET+ (Fig. 3C, middle) and with the PET0 patients (Fig. 3C, top). These Ki67-positive cells were mainly found in the adventitial immune infiltrates.

Inflammatory Infiltrate

The density and the nature of leukocytes were further characterized by immunostaining, and a semiquantification was performed in 6 pairs of samples from PET+ patients. The density of generic leukocytes (Supplemental Fig. 2), T lymphocytes (Fig. 4A), B lymphocytes (Fig. 4B), and plasmocytes (Fig. 4D) was significantly higher in the adventitia of the ^{18}F-FDG–positive site than in the negative site of the same patient. The density of macrophages ($CD68^+$) was also significantly higher in the positive sites (Fig. 4C) and mainly localized in the media and the inner adventitia. The density of generic leukocytes, T and B lymphocytes, and macrophages was significantly correlated with the rSUV (Supplemental Fig. 3) with a correlation coefficient of, respectively, 0.63, 0.62, 0.56, and 0.71.

Transcriptomic Analysis

The expression level of genes involved in extracellular matrix remodeling of the aortic wall (MMP1, 2, 3, 9, 12, 13, 14, and 15; TIMP [tissue inhibitor of MMP]; TIMP2; TIMP3; PAI1 [plasminogen activator inhibitor 1]; uPA [urokinase plasminogen activator]; RECK [reversion-inducing-cysteine-rich protein with kazal motifs]; and EMMPRIN [extracellular matrix metalloproteinase inducer]), in its maintenance and repair (COL1A1 [chain α 1 of collagen type 1], Elastin), in the inflammatory reaction (MCP1 [monocyte chimioattractant protein 1], IL1β, IL6, IL8, COX2 [cyclo-oxygenase 2], TNFα [tumor necrosis factor α], and TGFβ [transforming growth factor β]), in angiogenesis (HIF1α [hypoxia-inducible factor 1α, CD31, VEGF [vascular endothelial growth factor]), and a marker of SMC (α-SMA) was measured in the media and the adventitia collected in 5 PET0 patients and in 6 PET+ patients at the negative and positive sites. A complete listing of the results is given in Supplemental Tables 3 (media) and 4 (adventitia). The most striking differences are highlighted in Tables 4 and 5.

Comparison Between Negative Site of PET+ and PET0 Patients (Table 4). The expression level of the investigated genes in the media and adventitia was quite

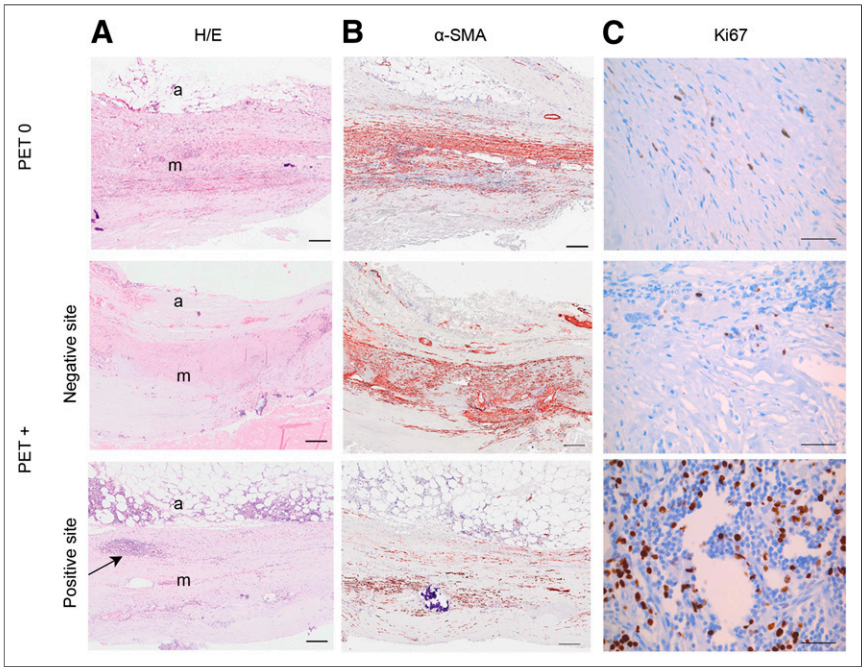

FIGURE 3. H/E staining (A), α-SMA immunostaining (B), and Ki67 immunostaining (C) of full-thickness sections from representative patients with negative PET (PET0) or with positive PET (PET+) at negative and positive site. Bar for H/E and α-SMA sections = 200 μm; bar for Ki67 sections = 50 μm. Arrow in A, bottom, points to tertiary lymphoid organ. a = adventitia; m = media.

TABLE 3
Inflammatory, α-SMA–positive, and Ki67-Positive Cell Quantification

Patient	Inflammatory infiltrate (AU)	α-SMA–positive cells (AU)	Ki67-positive cells (AU)
PET0			
Median	0.8	15.7	12.9
IQR	0.4–2.0	7.5–18.9	6.7–22.3
PET+/negative site			
Median	0.7	20.6	15.6
IQR	0.4–1.0	13.8–23.5	12.7–16.7
PET+/positive site*†			
Median	4.0	7.8	54.9
IQR	2.9–5.8	3.9–10.2	45.7–64.9

*$P < 0.05$ vs. PET0, Mann-Whitney *U* test.
†$P < 0.05$ vs. negative site of PET+, Wilcoxon signed-rank test.
IQR = interquartile range.

homogeneous in the population of PET0 patients, as indicated by the interquartile range, which is quite small for a human population (Supplemental Tables 3 and 4).

In the media, the expression of a series of genes (MMP12, MMP15, TIMP2, RECK, EMMPRIN, and type I collagen) was found significantly reduced in the metabolically inactive wall (negative site) of the PET+ group (Table 4) as compared with the PET0 patients. The chemokine IL8 was also significantly reduced whereas the other tested cytokines were unchanged. The proangiogenic markers did not differ between the 2 groups of samples. The metabolically inactive media from PET+ patients thus differs from that of PET0 patients by a reduced expression of genes involved in the extracellular matrix maintenance and remodeling and in the control of its degradation.

The adventitia of the negative site of the PET+ aneurysmal wall also significantly differed from the PET0 adventitia by a reduced expression of TNFα and TGFβ (Table 4). An increased expression—but quite variable among the PET+ patients precluding, therefore, statistical significance—was observed for IL6 and IL8.

Comparison Between Negative and Positive Site from Same Patient (Table 5). Some of the genes that were found reduced in the media of negative sites of the PET+ group, as compared with the PET0 media (i.e., TIMP2 and EMMPRIN), remained downregulated in the positive sites. By contrast, MMP1, MMP12, MMP13, TIMP1, and type I collagen expression was significantly increased (Table 5). The inflammatory cytokines and chemokines, such as MCP-1, IL1β, IL6, and COX2, were not altered whereas the TGFβ was significantly reduced. Elastin was also significantly reduced in the positive sites. These data suggest that an active remodeling of the matrix may take place in the media displaying a positive ^{18}F-FDG uptake.

This tendency was clearly strengthened in the positive adventitia, where 2 collagenases, MMP1 and MMP13, were strongly upregulated in all positives sites although the level of induction was highly variable between patients. Although MMP14, an activator of MMP2, and the plasminogen activator uPA were increased, the TIMPs, the physiologic inhibitors of many MMPs, remained constant or weakly reduced. The type I collagen messenger RNA level was strongly increased, by a factor of 5, as compared with the negative counterpart of the adventitia. Again, the inflammatory and angiogenic cytokines and chemokines were unchanged or even decreased, notably TGFβ and TNFα and VEGF (Table 5). These results show an increased expression of enzymes able to degrade the adventitial fibrillar collagen that would not be counterbalanced by their physiologic inhibitors accompanied by the implementation of a tentative compensatory repair process.

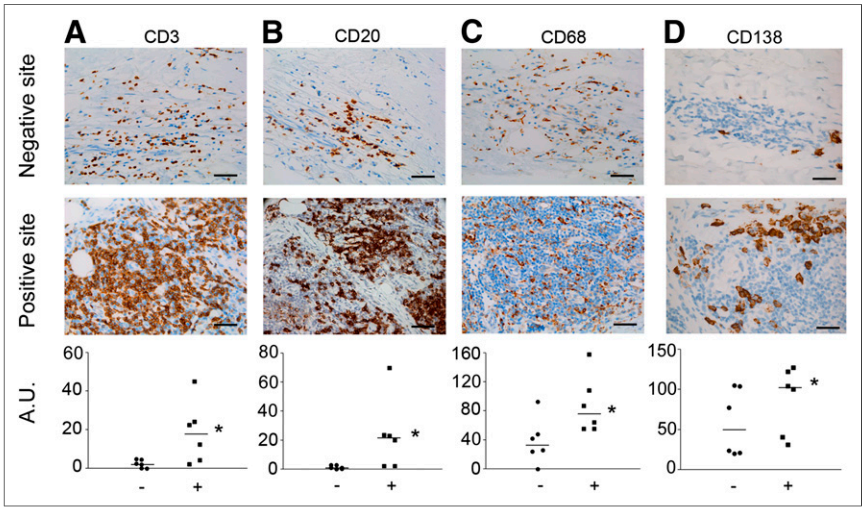

FIGURE 4. Immunolabeling of T lymphocytes (CD3, A), B lymphocytes (CD20, B), macrophages (CD68, C), and plasmocytes (CD138, D) in negative and positive sites of ^{18}F-FDG uptake from same patient. Semiquantifications were performed in 6 pairs of samples. *$P <$ 0.05, Wilcoxon signed-rank test. Bar = 50 μm.

Production and Activation of MMP2 and 9

MMP2 and MMP9 zymography of representative samples is illustrated in Supplemental Figure 4. In the media (Fig. 5A), the total amount of MMP9 was significantly increased in the positive sites as compared with their negative counterparts. A significantly higher proportion of activated enzyme (11%) was also observed as

TABLE 4
Modulated Genes at Negative Site of PET+ Patients Relative to PET0 Patients

Media		Adventitia	
Gene	Fold change	Gene	Fold change
MMP12	0.3*	TNFα	0.5*
IL8	0.3*	TGFβ	0.7*
MMP15	0.4*	IL8	2.5
RECK	0.5†	IL6	3.7
TIMP2	0.6*		
EMMPRIN	0.8†		
COL1A1	0.8*		

*$P < 0.05$, Mann–Whitney *U* test.
†$P < 0.01$, Mann–Whitney *U* test.
Results are expressed as median of fold changes relative to values measured in PET0 samples.

compared with the negative site (7%) and with the PET0 samples (0%). In the adventitia (Fig. 5B), the total amount of MMP2 was significantly increased in the positive sites as compared with their negative counterparts whereas the total amount of MMP9 was significantly increased in the positive sites as compared with the PET0 samples. Moreover, the proportion of activated form of MMP2 and MMP9 was significantly higher in the positive site of PET+ patients than of the PET0 group. A significantly higher activated MMP9 was also found in the negative adventitia of PET+ patients as compared with PET0.

DISCUSSION

Combined 3-dimensional metabolic imaging (^{18}F-FDG PET) and high-resolution anatomic pictures (CT) allowed the collection of biopsies of aneurysmal tissues specifically in the sites of positive ^{18}F-FDG uptake and in the metabolically inactive wall of the same patient. This original approach allowed a paired comparison in an aneurysm that has progressed in a single background of intrinsic and environmental factors. These paired biopsies were further compared with samples collected from AAA patients displaying no ^{18}F-FDG uptake, allowing the discrimination of systemic biologic alterations associated with ^{18}F-FDG uptake.

TABLE 5
Modulated Genes at Positive Site Relative to Negative Site of PET+ Patients

Media		Adventitia	
Gene	Fold change	Gene	Fold change
ELN	0.3*	EMMPRIN	0.7*
TIMP2	0.7*	VEGF	0.7*
EMMPRIN	0.8*	TIMP2	0.9*
TGFβ	0.8*	MMP14	1.6*
TIMP1	1.8*	TSP1	1.9*
MMP1	1.8*	uPA	2.2*
MMP12	1.8*	COL1A1	5.5*
COL1A1	2.2*	MMP13	9.1†
MMP13	3.9*	MMP1	12.9

*$P < 0.05$, Wilcoxon signed rank test.
†MMP13 was not detected in negative sites of PET+ adventitia; median value in positive site was calculated using lowest value as 1.
Results are expressed as median of fold changes relative to values measured in negative site of PET+ samples.

In agreement with our previous preliminary studies (*15,16*) and a recent report by Reeps et al. (*21*), the uptake of ^{18}F-FDG in the AAA wall was associated, in most patients, with symptomatic events such as accelerated growth and warning signals of potential rupture that were decisive factors for a surgical management. These observations are extended in the present study. It is worth noting that we were able to correlate the hot spots of ^{18}F-FDG uptake with high peak wall stress that, in some cases, corresponded to the point of rupture of the aneurysm (*22*).

The uptake of ^{18}F-FDG is likely related to the massive infiltrate of lymphocytes observed in the positive sites of the adventitia, which are probably activated as indicated by their increased proliferative activity and the increased number of plasmocytes. Moreover, macrophages present in the positive media in higher numbers may also incorporate ^{18}F-FDG as previously reported (*17*). The highly significant positive correlation between the SUV and the density of inflammatory cells strongly supports this assumption. The lymphocytes infiltrating AAA have indeed been characterized as activated memory cells (*23*). The formation of adventitial tertiary lymphoid organs in injured arteries is now characterized in the vascular rejection process, atherosclerosis, and AAA development (*6*) and has been sometimes correlated with chronic bacterial infections and autoimmune diseases (*24,25*). The adventitial tertiary lymphoid organs are mainly observed here in the positive ^{18}F-FDG uptake sites. Surprisingly, most of the cytokines tested in this study, except IL6 and IL8, were unchanged or even downregulated, such as TNFα. However, the investigation in future work of the chemokines involved in the recruitment of lymphocytes B and in adventitial tertiary lymphoid organ formation as described in rheumatoid arthritis would be beneficial (*26*).

The negative sites of the media of PET+ patients are characterized at the transcriptomic level by a reduced expression of genes involved in the extracellular matrix remodeling—such as type I collagen, various MMPs, and their physiologic inhibitors, TIMP2 and RECK—an observation potentially related to a lower metabolic activity of SMC. The significantly reduced expression of TGFβ is worth noting because its beneficial effect on AAA progression has been shown in animal models (*27,28*). Besides its antiinflammatory activity, TGFβ promotes SMC survival and matrix preservation. Its reduced expression in the negative site of the PET+ patients might preface aortic wall weakening.

One of the pathologic features of the PET+ patients is the significant reduction of α-SMA–positive cells in the media in the positive uptake site. This drastic reduction could be due to a higher rate of death of SMCs induced by a proteolytic and proapoptotic environment related to the massive infiltrate of leukocytes (*29*). Besides a significant increase and activation of 2 elastolytic enzymes (MMP2 and MMP9) as shown by zymography, the expression of MMP1, MMP13, MMP14, and their activator uPA was strikingly upregulated in the ^{18}F-FDG–positive adventitia as compared with the negative site of the same patient. In our study, MMP13 was never expressed in the adventitia of PET0 patients and only weakly present in the negative site of PET+ patients. MMP13 is one of the most potent collagenases characterized to date that can degrade many other extracellular matrix components

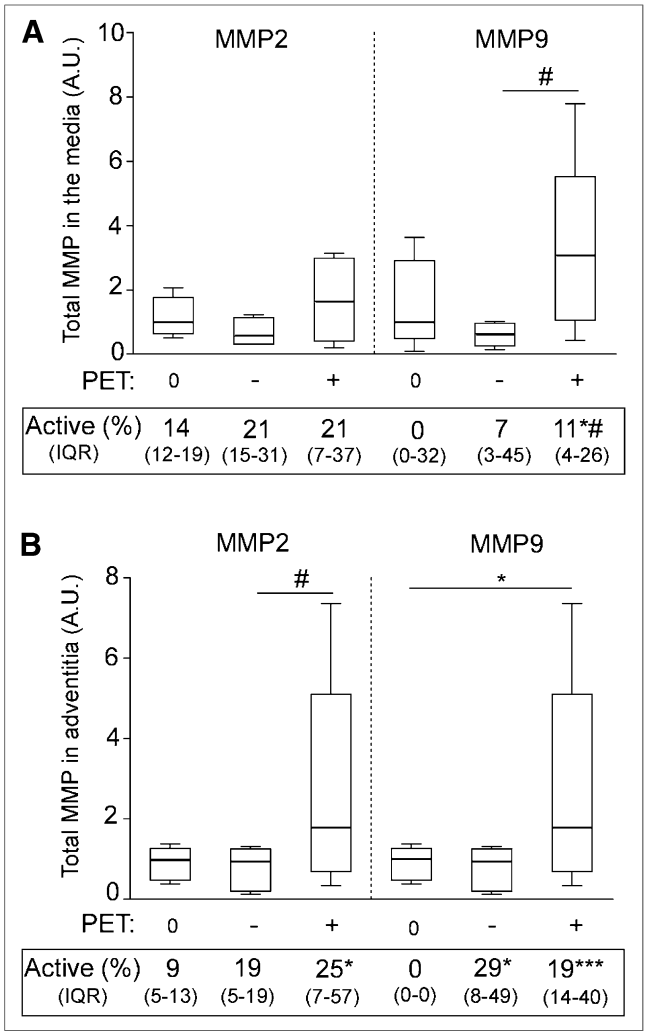

FIGURE 5. Quantification of MMP2 and MMP9 zymography analyses of samples collected from media and adventitia of PET0 patients (0) and PET+ patients at negative (−) or at positive site (+). Representative zymography gels are illustrated in Supplemental Figure 3. Box plot is of total MMP2 and MMP9 in media (A) and in adventitia (B). Median percentage of activated form is indicated below each group of samples (IQR). $^{*}P < 0.05$. $^{***}P < 0.001$ vs. PET0 samples, Mann–Whitney *U* test. $\#P < 0.05$, positive site vs. negative corresponding site, Wilcoxon signed-rank test. IQR = interquartile range.

(*30*). The expression of MMP13 is strictly regulated and often limited to situations of rapid remodeling; to conditions of chronic inflammation, such as rheumatoid arthritis; and to tumors. Its overexpression in the AAA wall in association with a predominance of B and T lymphocytes was also described (*31*). MMP1 and MMP13 may cooperate to degrade the adventitial fibrillar collagens type I and III that provide ultimate tensile strength to the aneurysmal aorta, resulting in a progressive weakening of the wall and finally its rupture. The largely upregulated expression of type I collagen in the positive adventitia is indicative of a tentative repair process by the resident adventitial cells. The accelerated growth rate observed in many of the PET+ patients suggests, however, a lack of efficiency of this process.

Altogether these data show that the ^{18}F-FDG uptake is likely related to the massive infiltrate of activated lymphocytes and macrophages in the aneurysmal wall, inducing a profound remodeling. They also present evidence that the aortic wall of PET+ patients presents molecular alterations as compared with PET0 patients. The modulation of a series of genes both in the negative and in the positive site of PET+ patients suggests that environmental events, such as bacterial infection, or systemic factors might affect the aneurysmal wall biology and activate pathways leading to wall degradation and accelerated growth. In agreement with this hypothesis, most PET+ patients presented a significantly higher preoperative circulating CRP level than the PET0 patients. A significant elevation of CRP in symptomatic patients (*32*) and a positive correlation between the circulating CRP and the expansion rate of AAA (*33*) have indeed been reported. Further work is needed to support this hypothesis.

A limitation of this study was the lack of direct evidence of coregistration of imaging data and biopsy collection in the positive ^{18}F-FDG uptake sites. However, the strong relationship between SUV and inflammatory infiltrate density argue in favor of a proper surgical sampling.

CONCLUSION

This study was undertaken to bring a large overview of the cellular and molecular alterations occurring in the metabolically active spots in the AAA wall. By investigating the metabolically inactive site in the same patient and comparing it with the aortic wall of PET0 patients, we disclosed significant differences suggesting that the whole aneurysmal wall might be affected by a general process. The metabolically active spots detected by the uptake of ^{18}F-FDG display striking alterations potentially related to medial degeneration and significant degradation of the fibrillar structures of the adventitia, which may ultimately lead to rupture. This study has disclosed several altered pathways that will require further investigations to identify markers relevant to rupture risk.

DISCLOSURE

The costs of publication of this article were defrayed in part by the payment of page charges. Therefore, and solely to indicate this fact, this article is hereby marked "advertisement" in accordance with 18 USC section 1734. This work was supported by the FP7 European Program "Fighting aneurysmal diseases" no. 200647, the Belgian Fonds de la Recherche Scientifique (grant no. 3.4518.07), and a grant from the University of Liège. No other potential conflict of interest relevant to this article was reported.

ACKNOWLEDGMENTS

We thank Audrey Hoffmann, Antoine Heyeres, and Emilie Feyereisen for their skillful technical assistance. The help of Emilie Delvenne for the histologic quantifications and of Nancy Garbacki for manuscript editing are acknowledged. We thank the surgeons and nurses of the Department of Cardiovascular and Thoracic Surgery of the CHU of Liège, the CHC St. Joseph, and CHR Citadelle for their contribution to the collection of AAA specimens.

REFERENCES

1. Sakalihasan N, Limet R, Defawe OD. Abdominal aortic aneurysm. *Lancet.* 2005;365:1577–1589.
2. Limet R, Sakalihassan N, Albert A. Determination of the expansion rate and incidence of rupture of abdominal aortic aneurysms. *J Vasc Surg.* 1991;14: 540–548.

3. Kurvers H, Veith FJ, Lipsitz EC, et al. Discontinuous, staccato growth of abdominal aortic aneurysms. *J Am Coll Surg.* 2004;199:709–715.
4. Powell JT, Gotensparre SM, Sweeting MJ, Brown LC, Fowkes FG, Thompson SG. Rupture rates of small abdominal aortic aneurysms: a systematic review of the literature. *Eur J Vasc Endovasc Surg.* 2011;41:2–10.
5. Georgakarakos E, Ioannou CV. Geometrical factors as predictors of increased growth rate or increased rupture risk in small aortic aneurysms. *Med Hypotheses.* 2012;79:71–73.
6. Michel JB, Thaunat O, Houard X, Meilhac O, Caligiuri G, Nicoletti A. Topological determinants and consequences of adventitial responses to arterial wall injury. *Arterioscler Thromb Vasc Biol.* 2007;27:1259–1268.
7. Sakalihasan N, Delvenne P, Nusgens BV, Limet R, Lapiere CM. Activated forms of MMP2 and MMP9 in abdominal aortic aneurysms. *J Vasc Surg.* 1996;24:127–133.
8. Liapis CD, Paraskevas KI. The pivotal role of matrix metalloproteinases in the development of human abdominal aortic aneurysms. *Vasc Med.* 2003;8:267–271.
9. Sakalihasan N, Heyeres A, Nusgens BV, Limet R, Lapiere CM. Modifications of the extracellular matrix of aneurysmal abdominal aortas as a function of their size. *Eur J Vasc Surg.* 1993;7:633–637.
10. Petersen E, Wagberg F, Angquist KA. Proteolysis of the abdominal aortic aneurysm wall and the association with rupture. *Eur J Vasc Endovasc Surg.* 2002;23:153–157.
11. Wilson WR, Anderton M, Schwalbe EC, et al. Matrix metalloproteinase-8 and -9 are increased at the site of abdominal aortic aneurysm rupture. *Circulation.* 2006;113:438–445.
12. Defawe OD, Colige A, Lambert CA, et al. Gradient of proteolytic enzymes, their inhibitors and matrix proteins expression in a ruptured abdominal aortic aneurysm. *Eur J Clin Invest.* 2004;34:513–514.
13. Sakalihasan N, Michel JB. Functional imaging of atherosclerosis to advance vascular biology. *Eur J Vasc Endovasc Surg.* 2009;37:728–734.
14. Rudd JH, Hyafil F, Fayad ZA. Inflammation imaging in atherosclerosis. *Arterioscler Thromb Vasc Biol.* 2009;29:1009–1016.
15. Sakalihasan N, Van Damme H, Gomez P, et al. Positron emission tomography (PET) evaluation of abdominal aortic aneurysm (AAA). *Eur J Vasc Endovasc Surg.* 2002;23:431–436.
16. Sakalihasan N, Hustinx R, Limet R. Contribution of PET scanning to the evaluation of abdominal aortic aneurysm. *Semin Vasc Surg.* 2004;17:144–153.
17. Defawe OD, Hustinx R, Defraigne JO, Limet R, Sakalihasan N. Distribution of F-18 fluorodeoxyglucose (F-18 FDG) in abdominal aortic aneurysm: high accumulation in macrophages seen on PET imaging and immunohistology. *Clin Nucl Med.* 2005;30:340–341.
18. Reeps C, Essler M, Pelisek J, Seidl S, Eckstein HH, Krause BJ. Increased ^{18}F-fluorodeoxyglucose uptake in abdominal aortic aneurysms in positron emission/computed tomography is associated with inflammation, aortic wall instability, and acute symptoms. *J Vasc Surg.* 2008;48:417–423.
19. Louis E, Ancion G, Colard A, Spote V, Belaiche J, Hustinx R. Noninvasive assessment of Crohn's disease intestinal lesions with ^{18}F-FDG PET/CT. *J Nucl Med.* 2007;48:1053–1059.
20. Paquet N, Albert A, Foidart J, Hustinx R. Within-patient variability of ^{18}F-FDG: standardized uptake values in normal tissues. *J Nucl Med.* 2004;45:784–788.
21. Reeps C, Bundschuh RA, Pellisek J, et al. Quantitative assessment of glucose metabolism in the vessel wall of abdominal aortic aneurysms: correlation with histology and role of partial volume correction. *Int J Cardiovasc Imaging.* 2013;29:505–512.
22. Xu XY, Borghi A, Nchimi A, et al. High levels of ^{18}F-FDG uptake in aortic aneurysm wall are associated with high wall stress. *Eur J Vasc Endovasc Surg.* 2010;39:295–301.
23. Ocana E, Bohorquez JC, Perez-Requena J, Brieva JA, Rodriguez C. Characterisation of T and B lymphocytes infiltrating abdominal aortic aneurysms. *Atherosclerosis.* 2003;170:39–48.
24. van de Pavert SA, Mebius RE. New insights into the development of lymphoid tissues. *Nat Rev Immunol.* 2010;10:664–674.
25. Gräbner R, Lotzer K, Dopping S, et al. Lymphotoxin beta receptor signaling promotes tertiary lymphoid organogenesis in the aorta adventitia of aged ApoE−/− mice. *J Exp Med.* 2009;206:233–248.
26. Manzo A, Paoletti S, Carulli M, et al. Systematic microanatomical analysis of CXCL13 and CCL21 in situ production and progressive lymphoid organization in rheumatoid synovitis. *Eur J Immunol.* 2005;35:1347–1359.
27. Wang Y, Ait-Oufella H, Herbin O, et al. TGF-beta activity protects against inflammatory aortic aneurysm progression and complications in angiotensin II-infused mice. *J Clin Invest.* 2010;120:422–432.
28. Dai J, Losy F, Guinault AM, et al. Overexpression of transforming growth factor-beta1 stabilizes already-formed aortic aneurysms: a first approach to induction of functional healing by endovascular gene therapy. *Circulation.* 2005;112:1008–1015.
29. Henderson EL, Geng YJ, Sukhova GK, Whittemore AD, Knox J, Libby P. Death of smooth muscle cells and expression of mediators of apoptosis by T lymphocytes in human abdominal aortic aneurysms. *Circulation.* 1999;99:96–104.
30. Leeman MF, Curran S, Murray GI. The structure, regulation, and function of human matrix metalloproteinase-13. *Crit Rev Biochem Mol Biol.* 2002;37:149–166.
31. Reeps C, Pelisek J, Seidl S, et al. Inflammatory infiltrates and neovessels are relevant sources of MMPs in abdominal aortic aneurysm wall. *Pathobiology.* 2009;76:243–252.
32. Domanovits H, Schillinger M, Mullner M, et al. Acute phase reactants in patients with abdominal aortic aneurysm. *Atherosclerosis.* 2002;163:297–302.
33. De Haro J, Acin F, Bleda S, Varela C, Medina FJ, Esparza L. Prediction of asymptomatic abdominal aortic aneurysm expansion by means of rate of variation of C-reactive protein plasma levels. *J Vasc Surg.* 2012;56:45–52.